# Crystal Structures of the *Helicobacter pylori* MTAN Enzyme Reveal Specific Interactions between *S*-Adenosylhomocysteine and the 5′-Alkylthio Binding Subsite

Vidhi Mishra and Donald R. Ronning*

Department of Chemistry, University of Toledo, Toledo, Ohio 43606, United States

ABSTRACT: The bacterial 5′-methylthioadenosine/*S*-adenosylhomocysteine nucleosidase (MTAN) enzyme is a multifunctional enzyme that catalyzes the hydrolysis of the *N*-ribosidic bond of at least four different adenosine-based metabolites: *S*-adenosylhomocysteine (SAH), 5′-methylthioadenosine (MTA), 5′-deoxyadenosine (5′-DOA), and 6-amino-6-deoxyfutalosine. These activities place the enzyme at the hub of seven fundamental bacterial metabolic pathways: *S*-adenosylmethionine (SAM) utilization, polyamine biosynthesis, the purine salvage pathway, the methionine salvage

pathway, the SAM radical pathways, autoinducer-2 biosynthesis, and menaquinone biosynthesis. The last pathway makes MTAN essential for *Helicobacter pylori* viability. Although structures of various bacterial and plant MTANs have been described, the interactions between the homocysteine moiety of SAH and the 5′-alkylthiol binding site of MTAN have never been resolved. We have determined crystal structures of an inactive mutant form of *H. pylori* MTAN bound to MTA and SAH to 1.63 and 1.20 Å, respectively. The active form of MTAN was also crystallized in the presence of SAH, allowing the determination of the structure of a ternary enzyme—product complex resolved at 1.50 Å. These structures identify interactions between the homocysteine moiety and the 5′-alkylthiol binding site of the enzyme. This information can be leveraged for the development of species-specific MTAN inhibitors that prevent the growth of *H. pylori*.
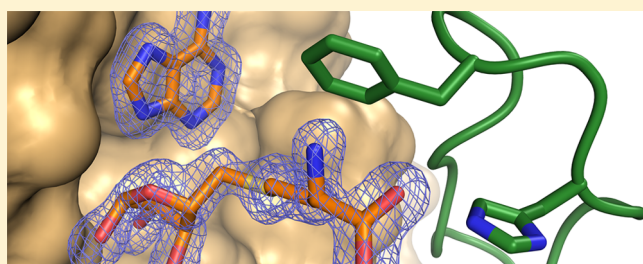
5′-Methylthioadenosine/*S*-adenosylhomocysteine nucleosidase plays a key role in multiple pathways in bacterial cells. It catalyzes the hydrolysis of the *N*-ribosidic bond of four different adenosine-based metabolites, releasing adenine and the ribose-containing products (Figure 1). It has been known that it utilizes SAH, MTA, and 5′-DOA from the various SAM utilization pathways.[1−3] SAH is a product of every SAM-dependent methyl transfer reaction. These biochemical transformations encompass methylation of the three common biological polymers (proteins, nucleic acids, and complex carbohydrates) as well as various lipids.[4] Methylation of these polymers affects fundamental properties in all living organisms such as gene expression, cell signaling, and cellular metabolism. In all of these cases, SAM-dependent methylation is susceptible to product inhibition if SAH accumulates to high levels.[5] Continuous breakdown of MTA is also required for the proper functioning of spermidine and spermine synthases that are otherwise inhibited by the accumulation of MTA.[6] MTAN activity is also linked to important downstream metabolic pathways such as adenine and methionine salvage and autoinducer I (AI1) and II (AI2) production, which are important quorum-sensing signaling molecules.[7] AI2 regulates the expression of genes that are required for interspecies communication, biofilm formation, and bacterial virulence and are therefore important facilitators of bacterial pathogenesis.[8,9] The AI2 concentration in the cell depends on the transformation of *S*-ribosylhomocysteine (SRH) into homocysteine

and 4,5-dihydroxy-2,3-pentanedione, a precursor of AI2.[10] AI1 compounds are *N*-acylhomoserine lactones (AHLs) that allow intraspecies communication in primarily Gram-negative bacteria. AHL synthase catalyzes the transformation of SAM into AHL and MTA, so the activity of AHL synthase is sensitive to the accumulation of MTA.[11] Choi-Rhee and Cronan have reported that MTAN is required for the catalytic hydrolysis of 5′-DOA and that accumulation of 5′-DOA inhibits SAM radical enzymes such as biotin synthase.[1] Recently, Li et al. determined that the *Campylobacter jejuni* and *Helicobacter pylori* MTAN (*Hp*MTAN) enzymes play an essential role in an alternative menaquinone biosynthetic pathway.[12] They reported that, unlike *Escherichia coli* and *Thermus thermophillus*, *C. jejuni* and *H. pylori* biosynthesize menaquinone though an intermediate step that requires MTAN to catalyze the hydrolysis of 6-amino-6-deoxyfutalosine. This role, combined with previous data, suggests that MTAN represents a target for compounds capable of affecting bacterial metabolism and bacterial communication.[7,13,14] Indeed, very recently, Wang et al. have shown that powerful inhibitors of MTAN inhibit the growth of *H. pylori*.[15]

Previously determined bacterial and plant MTAN structures show that MTAN is an obligatory homodimer, and the two molecules form a set of two shared active sites where residues
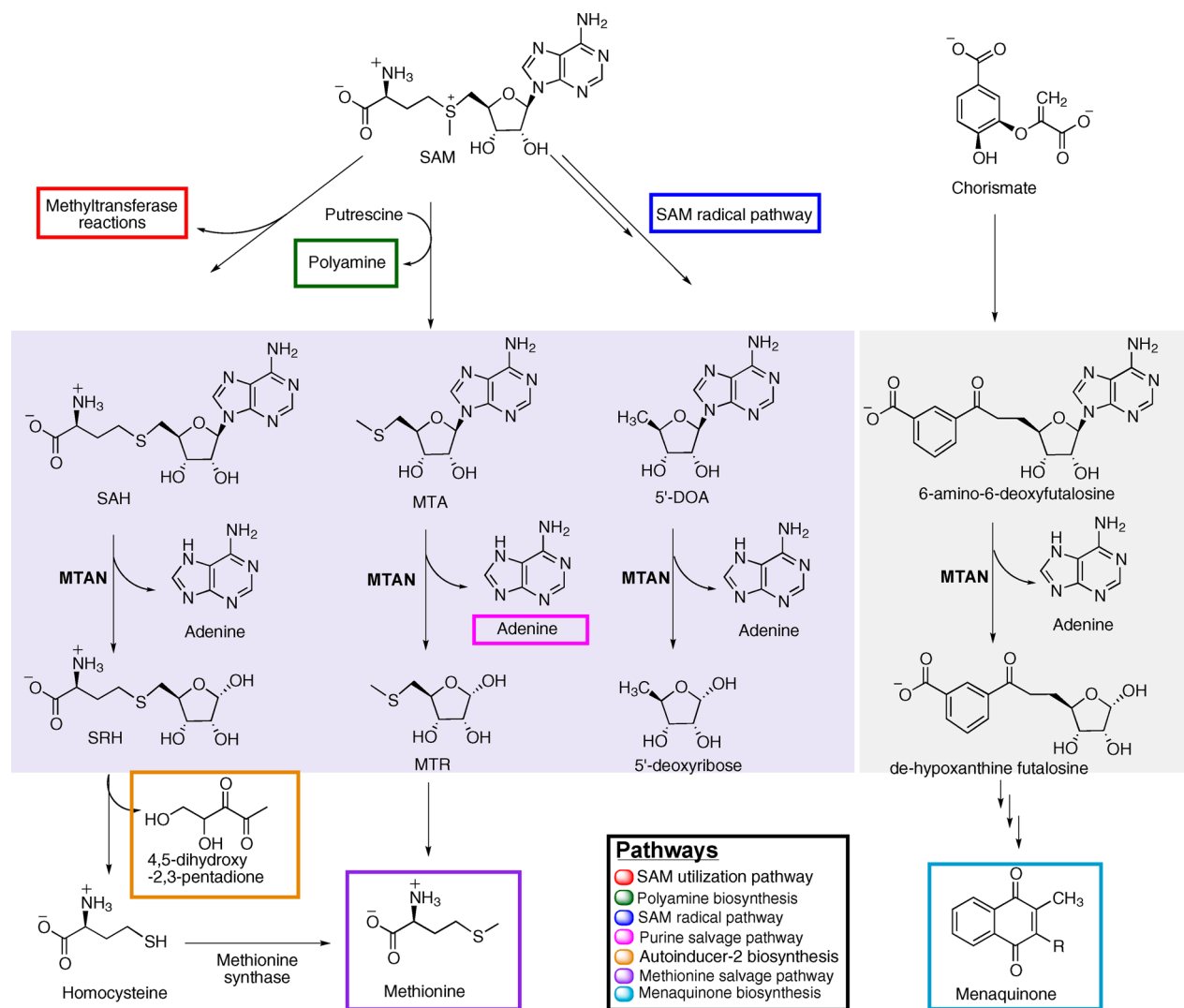
Figure 1. MTAN is a multifunctional enzyme. MTAN has been shown to use three different adenosine-based substrates in diverse bacterial systems: SAH, MTA, and 5′-DOA (light violet background). In *Campylobacter*, it also hydrolyzes the *N*-ribosidic bond of 6-amino-6-deoxyfutalosine (gray background). Colored boxes encompass the compounds relevant to the pathways directly affected by MTAN activity. Only one adenine is boxed, but all four MTAN-catalyzed reactions allow adenine salvage.

of one molecule form the adenyl and ribosyl binding pockets and residues of the other molecule form the majority of the 5′-alkylthio binding pocket (Figure 2A).[16−19] The catalytic mechanism has been thoroughly characterized as well as the interactions required to initiate that reaction (Figure 2B,C).[20−23] Binding of the substrate to the open form of the enzyme stimulates a conformational change characterized predominately by the kinking of helix α6. This closes the active site and positions residue D198 (*Hp*MTAN numbering) to interact with N7 and the N6 exocyclic amine of the adenine moiety. It has been suggested that D198 acts as a general acid by donating a proton to N7 of the substrate, resulting in the stretching of the *N*-ribosyl bond and subsequent formation of an oxocarbenium intermediate that undergoes nucleophilic attack by a water molecule.[16] Release of the adenine and SRH products appears to be facile following hydrolysis and relaxation of helix α6.

Although much is known about the structure of MTAN and its interactions with adenosine-containing substrates, specifically inhibiting the bacterial MTANs without also inhibiting homologous human enzymes is a challenge. The human genome encodes both a purine nucleoside phosphorylase and the 5′-MTA phosphorylase (MTAP) that are inhibited by the current generation of MTAN inhibitors.[24,25] The MTAN inhibitors with the tightest binding are either transition-state or nucleoside analogues that interact with residues forming the ribosyl and adenyl binding pockets within the active site.[22,26] These regions are largely conserved between the bacterial MTANs and MTAPs.[16] As a result, some of these compounds possess lower K_i values for human MTAP than for MTAN.[27] Comparison of the MTAN and MTAP active site structures shows that the latter possesses a truncated 5′-alkylthio binding pocket that permits use of MTA as a substrate but not SAH.[28] Because the larger 5′-alkylthio binding subsite of MTAN is an important feature that differentiates it from human MTAP, characterization of the specific interactions between the 5′-alkylthio binding site of MTAN and the homocysteine moiety of SAH may offer insight into the design of MTAN inhibitors with improved selectivity for the bacterial enzymes as a basis for new drugs for the treatment of *H. pylori* infections.
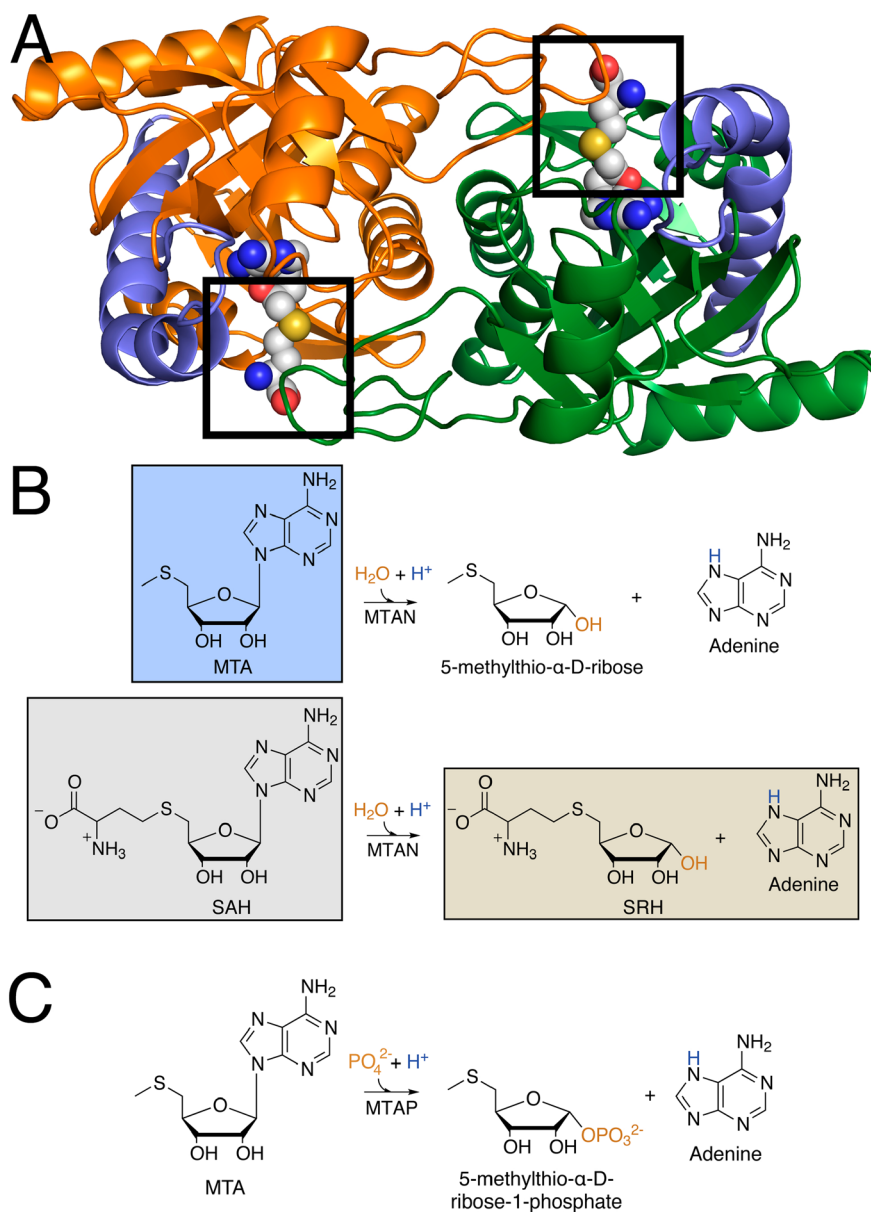
Figure 2. Shared active site in the *Hp*MTAN homodimer and the enzyme mechanism. (A) The closed form of the *Hp*MTAN-D198N active site is shown with SAH (spheres colored by CPK) bound. The cartoons (orange and green) represent the *Hp*MTAN homodimer. The position of helix α6 is indicated for each monomer in light blue. The boxed regions indicate the location of the 5′-alkylthio binding subsite that interacts with the homocysteine moiety of SAH. (B) Reactions proposed for the two most commonly studied MTAN substrates. The ligands for each of the determined structures are highlighted in boxes. The substrates are colored black; the nucleophile is colored orange, and the MTAN-derived proton is colored blue. (C) Proposed reaction for the human MTAP enzyme. The coloring of the components is the same as in panel B.
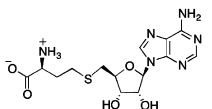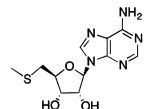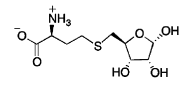
EXPERIMENTAL PROCEDURES

Mutagenesis. Site-directed mutagenesis was performed to make the D198N mutant using a pET-32-based plasmid containing the wild-type *pfs* gene as a template. The template plasmid encodes a polyhistidine-tagged thioredoxin−*Hp*MTAN fusion protein containing a Prescission protease cut site immediately N-terminal to the first residue of wild-type *Hp*MTAN (wt-*Hp*MTAN). Proteolysis with Prescission protease produces a polyhistidine-tagged thioredoxin and untagged *Hp*MTAN. Sequencing of the plasmid resulting from the mutagenesis experiment confirmed the presence of the D198N mutation.

MTAN Expression and Purification. Wild-type *Hp*MTAN and its mutants were expressed and purified as previously described.[18] The plasmid containing the mutated gene was used to transform BL21(DE3) Rosetta cells (EMD Biosciences). Cultures of LB medium containing 0.1 mM chloramphenicol and 0.3 mM ampicillin were incubated at 37 °C. Cells were induced after Abs_{600} had reached 0.6−0.8 by the addition of 0.1 mM IPTG and incubated for 18−20 h at 16 °C. Cells were harvested by centrifugation and resuspended in buffer A [20 mM HEPES (pH 7.5), 0.5 M NaCl, 5 mM β-mercaptoethanol, and 25 mM imidazole]. The resuspended cells were lysed by sonication and then centrifuged at 15000*g*. The supernatant was applied to a 5 mL HisTrap column equilibrated with buffer A (GE Healthcare). Elution of recombinant proteins was performed using a linear gradient of imidazole from 25 to 250 mM over 20 column volumes. The fractions containing the purified proteins were treated with Prescission Protease and

Table 1. X-ray Diffraction and Refinement Statistics[a]

	MTAN-D198N/SAH	MTAN-D198N/MTA	wt-MTAN/SRH/adenine
Resolution range (Å) [highest shell]	50.00-1.20 [1.22-1.20]	50.00-1.63 [1.67-1.63]	50.00-1.50 [1.53-1.50]
Space group	P3$_2$21	P3$_2$21	P3$_2$21
a, b (Å)	80.7	80.7	81.2
c (Å)	67.2	67.2	67.4
Total reflections [unique reflections]	822470 [75266]	348061 [32308]	237786 [40655]
Completeness (%) [highest shell]	95.0 [92.6]	99.7 [99.2]	98.5 [97.5]
Redundancy [highest shell]	10.9 [10.7]	10.8 [10.1]	5.8 [5.7]
Average I/σ (I) [highest shell]	16.0 [4.1]	11.7 [3.3]	13.9 [3.6]
R$_{sym}$ (%) [highest shell]	5.0 [30.0]	6.5 [38.1]	6.2 [44.9]
Atoms/A.S.U	2,218	2,127	2,010
R$_{work}$ (%)	15.4	13.5	18.2
R$_{free}$ (%)	17.5	17.8	20.5
Average B-factor protein (Å^2)	16.6	20.9	22.2
Average B-factor ligand (Å^2)	14.1	18.9	21.3
Average B-factor solvent (Å^2)	27.0	31.3	29.5
Ligand occupancy (%)	100	100	100
r.m.s. bonds (Å)	0.005	0.005	0.006
r.m.s. angles (°)	1.09	0.95	0.99
Ramachandran favored (%)	96.9	96.9	96.9
Ramachandran disallowed (%)	0.0	0.0	0.0
Coordinate Error (Å)	0.14	0.17	0.34

[a]The structures of the enzyme-bound compound are shown for the sake of clarity. Parentheses indicate units. Brackets indicate additional information regarding that value. A.S.U means asymmetric unit; r.m.s. means root-mean-square. $R_{sym} = \sum |I_i - \langle I_i \rangle| / \sum |I_i|$, where I is the intensity of a given reflection and $\langle I \rangle$ is the average intensity for that reflection. R_{work} and $R_{free} = \sum ||F_o| - |F_c|| / \sum |F_o|$, where F_o and F_c are the observed and calculated structure factor amplitudes, respectively. R_{free} is calculated from a set of reflections chosen randomly. These data are equal to 5% of the unique reflections and were not used for model refinement or calculation of the R_{work} value.

dialyzed overnight against buffer A. This protein sample was again applied to a HisTrap column (GE Healthcare) to selectively bind the cleaved histidine tag and the protease. The fractions containing *Hp*MTAN were then subjected to size exclusion chromatography on a Hi-Load Superdex 200 column as a polishing step (GE Healthcare). All protein samples were analyzed for purity using sodium dodecyl sulfate−polyacrylamide gel electrophoresis. The absorbance at 280 nm was used to determine the protein concentration using an extinction coefficient of 3105 M^{-1} cm^{-1}.

Crystallization. For the crystallization studies, purified protein samples were dialyzed against crystallization buffer [20 mM HEPES (pH 7.5), 0.2 mM TCEP, and 1 mM EDTA] and concentrated to 16 mg/mL by ultrafiltration (Millipore). Crystals of the MTAN-D198N mutant complexed with either MTA or SAH were grown by the hanging-drop vapor diffusion method. Crystallization drops containing 1 μL of well solution, 1 μL of MTAN-D198N (16 mg/mL), and 0.5 μL of SAH or MTA (10 mM) were equilibrated with 100 μL of well solution. The well solution for producing MTAN-D198N−MTA complex crystals contained 0.2 M magnesium chloride, 0.1 M HEPES (pH 7.5), and 25% (w/v) PEG 3350. The well solution for producing the MTAN-D198N−SAH complex crystals contained 0.05 M magnesium chloride hexahydrate, 0.1 M HEPES (pH 7.5), and 30% (v/v) PEG-MME 550. Crystals of the wt-*Hp*MTAN−SRH−adenine complex were produced under the same conditions as the MTAN-D198N−SAH complex crystals. X-ray diffraction experiments were performed on the LS-CAT ID-D beamline at the Advanced Photon Source (Argonne National Laboratory, Argonne, IL). Data were integrated and scaled using HKL2000.[29] Although these crystals were isomorphous with previously determined *Hp*MTAN structures, molecular replacement was necessary and performed with a monomer of *Hp*MTAN [Protein Data Bank (PDB)

entry 3NM6] using EPMR.[30] Structure refinement proceeded using Phenix and Coot.[31−33]

Kinetic Characterization of wt-MTAN. All assays were performed in triplicate in 100 mM HEPES and 50 mM KCl buffer (pH 7.2). For determining kinetic parameters, stocks of 1 mM SAH and 1 mM MTA were prepared in the same buffer. The substrates were serially diluted to produce a final concentration range of 5−150 μM in 100 μL of assay solution. The reduction of absorbance at a wavelength of 274 nm was monitored for 15 min at 37 °C using a Biotek (Winooski, VT) Synergy H4 plate reader. The extinction coefficient of 1.6 mM^{-1} cm^{-1} was used for assays with both SAH and MTA. Nonlinear regression analysis of kinetic data was performed using Prism 5.

■ RESULTS AND DISCUSSION

The Homocysteine Moiety of SAH Forms Specific Interactions with the *Hp*MTAN Active Site. Although much is known about the interactions between MTAN and the adenosine moiety of the variety of functional substrates, the mechanism by which MTAN interacts with components of the 5′-alkylthio moiety of those substrates is not. The strategy used to characterize these interactions was to create an inactive mutant capable of binding substrate but lacking enzymatic activity. On the basis of the previously reported *E. coli* MTAN (*Ec*MTAN) mutant−MTA complex, an *Hp*MTAN-D198N mutant was created.[23] The crystal structure of the *Hp*MTAN-D198N−SAH complex was determined and refined to 1.2 Å resolution (Table 1), allowing for clear assessment of the interactions between the SAH substrate and the 5′-alkythio binding subsite.

The difference maps within the region enveloped by the *Hp*MTAN-D198N active site exhibited electron density that allowed unambiguous fitting of each non-hydrogen atom of
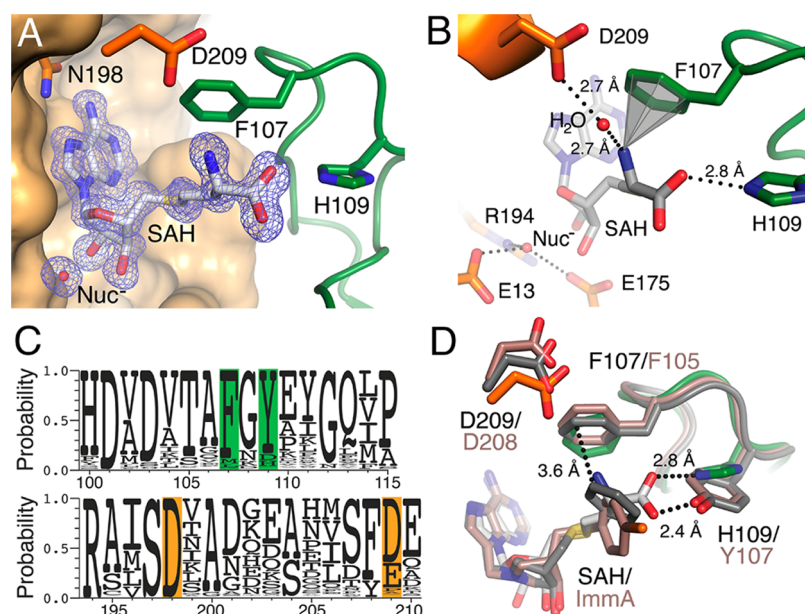
Figure 3. SAH active site interactions. (A) *Hp*MTAN-D198N active site. The electron density of an $F_o - F_c$ omit map is shown contoured at 3σ, where both SAH and the nucleophilic water (Nuc⁻) were omitted during map calculation. The orange molecular surface represents most of *Hp*MTAN-D198N molecule 1 with the exception of residues N198 and D209 (shown with orange carbons). N198 is the residue mutated to inactivate the enzyme. The green ribbon and carbon atoms correspond to molecule 2 of the homodimer, with residues F107 and H109 forming direct interactions with the substrate. Heteroatoms are colored by CPK. (B) Colors are as indicated for panel A. Dashed lines indicate bonding interactions. The gray cone signifies the cation−π interaction. The nucleophilic water and the conserved residues that coordinate it are positioned at the bottom left and labeled. (C) Sequence alignment of 1000 MTAN sequences shown as a logo alignment. Residues are numbered according to that of *Hp*MTAN. The orange background indicates important residues originating from molecule 1, and the green background highlights those originating from molecule 2. (D) Superposition of the wt-*Ec*MTAN−Immucillin and *Hp*MTAN-D198N−SAH complexes highlights the interactions within the 5′-alkylthio binding subsite. The atoms of the *Hp*MTAN-D198N−SAH complex are as shown previously. The dark gray atoms indicate those from the wt-*Ec*MTAN−BnT-DADMeImmA complex (PDB entry 3DF9), while the rose-colored atoms represent those from the wt-*Ec*MTAN−(4-chlorophenyl)thio-DADMe-Immucillin-A complex (PDB entry 3O4V). The rose labels indicate residues from wt-*Ec*MTAN−inhibitor complexes, while black labels indicate residues from the *Hp*MTAN-D198N−SAH complex. The potential hydrogen bond between the α-carboxyl of SAH and Y107 of *Ec*MTAN is shown as a dashed bond with a length of 2.4 Å. The interaction between BnT-DADMe-Immucillin and F105 of *Ec*MTAN is shown as a dashed bond with a length of 3.6 Å.

SAH, including the previously unobserved α-amino and carboxyl groups of the homocysteine moiety (Figure 3A). The α-amino group of the homocysteine moiety forms two types of interactions with the 5′-alkythio binding subsite. The first is a cation−π interaction with the aromatic side chain of F107, which is positioned 3.3 Å from the α-amino nitrogen of SAH and the six carbons of the phenylalanine aromatic ring (Figure 3B). This type of interaction has been observed in other proteins that specifically bind ligands or substrates that contain ammonium moieties, and disruption of the cation−π interaction is known to affect the binding affinity within those systems.[34] Excellent examples of this are represented by the structures of the γ-aminobutyric acid (GABA) receptor and acetylcholine binding protein (AChBP) bound to their respective ligands or ligand analogues.[34−36] In the AChBP−carbamylcholine structure, the aromatic residues found within the AChBP ligand binding pocket form multiple cation−π interactions with the quaternary ammonium of carbamylcholine.[35] Recently, this type of interaction was observed in an insect GABA receptor, and incorporation of artificial fluorophenylalanine amino acids within the ligand binding site of the acetylcholine receptor eliminates a cation−π interaction and produces a consistent increase in the measured EC_{50} values when compared to that of the wild-type acetylcholine receptor.[34]

The second interaction between *Hp*MTAN-D198N and the α-amino moiety occurs through a water-mediated hydrogen

bond to D209. This residue is located near the N-terminus of helix α6, which is disordered in ligand-free MTAN structures but takes a helical form as a consequence of substrate binding.[18,23] One consequence of this structural organization is the positioning of D198 near the adenyl moiety to initiate the transfer of a proton to the substrate, while the other consequence is the formation of the through-water hydrogen bond. The distances from the water molecule to the side chain of D209 and to the α-amino moiety of SAH are equal, with each hydrogen bond measuring 2.7 Å (Figure 3B). Additionally, the 4.4 Å distance between the side chain of D209 and the α-amino moiety of SAH suggests a possible ionic interaction. The α-carboxyl moiety of SAH in the *Hp*MTAN-D198N−SAH complex also forms a specific interaction with the enzyme active site. Specifically, the Nε atom of H109 forms a 2.8 Å bonding interaction with SAH.

To assess the potential importance of these interactions in substrate recognition, we performed a sequence alignment of the 1000 MTAN protein sequences in the UniProt database most closely related to that of *H. pylori* (Figure 3C). This sequence comparison showed that more than 85% of these MTANs possess a phenylalanine at the position corresponding to F107 in *Hp*MTAN, suggesting that the cation−π interaction is an important feature that supports specific enzyme−substrate interactions. The sequence alignment also suggests that the charge of the residue at position 209 is important, as it is either an aspartate or glutamate in roughly 90% of the 1000 analyzed
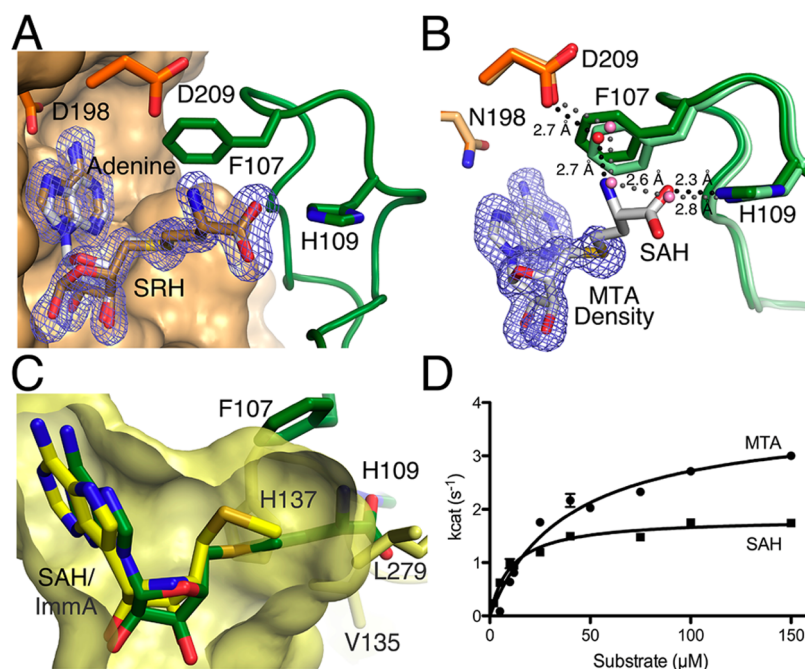
Figure 4. Comparison of SAH and MTA as substrates. (A) Superposition of the *Hp*MTAN-D198N−SAH and wt-*Hp*MTAN−SRH−adenine complex structures. The $F_o − F_c$ difference density from the wt-*Hp*MTAN−SRH−adenine diffraction data is shown contoured at 3σ. Both SRH and adenine were omitted from the calculation of the map. The coloring of the protein and SAH is the same as in the other figures. The bronze carbon atoms represent the SRH and adenine products. (B) Superposition of the *Hp*MTAN-D198N−SAH and −MTA complex structures. The protein atoms from the *Hp*MTAN-D198N−SAH structure are colored as in the other figures, and the carbon atoms of the enzyme of the MTA complex structure are slightly lighter in color. Because SAH and MTA atom positions superimpose perfectly, the atoms of MTA are not shown, but the location of MTA is indicated by an $F_o − F_c$ omit map contoured at 3σ where MTA was omitted from the calculation of the map. The hydrogen-bonded water network in the MTA-bound structure is indicated by the dashed gray lines, and that of the SAH complex structure is indicated by the dashed black lines. (C) *Hp*MTAN and human MTAP 5′-alkylthio binding subsites differ in structure. A superposition of the *Hp*MTAN-D198N−SAH complex active site with the human MTAP active site showing bound methylthio-Immucillin-A (PDB entry 1K27). Components of the *Hp*MTAN-D198N−SAH complex are colored as in the other figures. The corresponding 5′-alkylthio binding subsite of human MTAP is colored yellow. The yellow carbon atoms and surface indicate the MTAP−methylthio-Immucillin-A (ImmA) complex and the active site cavity, respectively. H137, V135, and L279 form the boundary of the 5′-alkylthio binding subsite in MTAP. H109, F107, and SAH of the *Hp*MTAN-D198N−SAH complex are also shown. The homocysteine moiety of SAH protrudes more than 4 Å beyond the confines of the human MTAP active site. (D) Comparison of steady-state kinetics using either MTA or SAH shows a slightly higher affinity for SAH but a lower rate of enzyme turnover when compared to those with MTA. Error bars are the result of reactions performed in triplicate.

MTAN sequences. If any hydrogen bond acceptor or donor were sufficient at this position, one would expect to observe asparagine and glutamine with roughly equivalent probabilities. H109 is conserved in bacteria of the order Campylobacterales, which represents approximately 10% of the 1000 MTAN sequences inspected in this study. In contrast, 80% of the sequences possess a tyrosine residue at the analogous position, which is common to all of the previously determined bacterial MTAN structures. Superposition of *Hp*MTAN with *Ec*MTAN (Figure 3D) suggests that a tyrosine side chain could maintain a hydrogen bond with the α-carboxyl of SAH. This highlights the importance of MTAN possessing a hydrogen bond donor or acceptor at this position. In addition, the lack of a resolved SAH−MTAN complex prior to this study suggests that a hydrogen bond between the tyrosine of *Ec*MTAN and the SAH α-carboxylate is insufficient to structurally resolve this interaction, whereas the interaction between the α-carboxyl moiety of SAH and H109 of *Hp*MTAN-D198N is sufficiently strong to fix the conformation of SAH. To ensure that these interactions are observed in the wild-type enzyme and to identify any structural changes in the 5′-alkylthio binding region following substrate hydrolysis, we determined the crystal structure of wt-*Hp*MTAN complexed with adenine and SRH to 1.50 Å resolution.

Active Site Interactions with the Homocysteine Moiety Are Unchanged during Catalysis. Previous attempts to form a wt-MTAN−product complex resulted in a complex with adenine and Tris in the active site.[18] The crystallization experiments described here produced wt-MTAN crystals in the closed form with both adenine and the α-anomer of SRH bound in the active site as evidenced by two discrete regions of density in an $F_o − F_c$ difference map (Figure 4A). The presence of the α-anomer is consistent with the proposed catalytic mechanism in which breaking of the *N*-ribosidic bond produces an oxocarbenium intermediate that undergoes a nucleophilic attack on the α-face of the ribosyl group. This nucleophilic attack is from an ordered water molecule coordinated by conserved residues E13, E175, and R194, which has been observed in all MTAN crystal structures to date (Figure 3B).[16,18] In the wt-*Hp*MTAN−SRH−adenine structure, it is clear that conversion from the β-ribosyl substrate to the α-ribosyl product also alters the ribose conformation from $C_{4'}$-endo to $C_{2'}$-endo. This stems from maintaining the location of the nucleophilic water, which is now O1 of the SRH product, through continued coordination by residues E13, E175, and R194. This conformational change in the ribosyl moiety contrasts with the fixed conformation of the homocysteine moiety and the interactions it forms with the 5′-alkylthio

Table 2. *Hp*MTAN Kinetic Parameters

	SAH			MTA		
	K_M (μM)	k_{cat} (s^{-1})	k_{cat}/K_M (μM^{-1} s^{-1})	K_M (μM)	k_{cat} (s^{-1})	k_{cat}/K_M (μM^{-1} s^{-1})
wt	10 ± 1	1.8 ± 0.1	0.17 ± 0.02	39 ± 5	3.8 ± 0.2	0.097 ± 0.009
F107A	19 ± 3	0.44 ± 0.02	0.023 ± 0.002	37 ± 4	1.0 ± 0.1	0.027 ± 0.002
H109A	14 ± 4	0.74 ± 0.05	0.051 ± 0.010	33 ± 6	1.2 ± 0.1	0.037 ± 0.004

binding pocket. This suggests that interactions defined by the 5′-alkylthio binding subsite allow for less conformational flexibility than those in the ribose binding subsite and that the interactions between the homocysteine moiety and the 5′-alkythio binding subsite likely remain unchanged throughout the enzymatic reaction.

The *Hp*MTAN 5′-Alkylthio Binding Subsite Structure Is Substrate-Independent. The first X-ray crystal structures of MTAN highlighted the conformational change in helix α6 resulting from the induced fit between MTAN and its substrates. However, inspection of the 5′-alkylthio binding subsites from the published MTAN structures suggests that this region is insensitive to the substrate-bound state of the enzyme. To determine if the variability of the 5′-alkylthio moieties of the known MTAN substrates affects differences in the structure of the 5′-alkylthio binding subsite, we determined the crystal structure of an *Hp*MTAN-D198N–MTA complex to 1.6 Å resolution and compared this structure to the *Hp*MTAN–D198N–SAH complex structure.

When superimposing the MTA and SAH complex structures (root-mean-square displacement for Cα atoms of 0.067 Å), the MTA substrate superimposes perfectly with the corresponding atoms of SAH. Additionally, the 5′-alkylthio binding pockets of both structures maintain the same conformation (Figure 4B). In particular, the loop containing residues F107 and H109 maintains the identical conformation in both structures. Other similarities between the SAH and MTA complexes are the solvent structure and the hydrogen-bonded network within the 5′-alkylthio binding pocket. Specifically, the hydrogen-bonded network formed by D209, a water molecule, and the α-amino group of SAH is observed in the MTA structure as a D209–water–water network. These solvent interactions and the lack of structural changes in the 5′-alkylthio binding pocket suggest that MTAN follows a lock-and-key model for binding the homocysteine moiety that contrasts with the dynamics observed in the residues that form the adenyl and ribosyl binding sites.[37] On the basis of the findings described here, it is possible to draw parallels between the interactions observed in the *Hp*MTAN-D198N–SAH complex and those interactions likely formed in a complex of the *Hp*MTAN with the recently identified MTAN substrate, 6-amino-6-deoxyfutalosine. Primarily, the benzoate moiety of 6-amino-6-deoxyfutalosine would be positioned like the α-amino group of SAH within the 5′-alkylthio binding subsite and interact with F107 through a π–π stacking interaction. Because 6-amino-6-deoxyfutalosine, like SAH, terminates with a carboxylate moiety, it likely forms an interaction with H109 similar to that observed in the *Hp*MTAN-D198N–SAH and wt-*Hp*MTAN–SRH–adenine complexes.

To date, two wt-MTAN complex structures have been determined with a ligand containing an aromatic functional group bound within the 5′-alkylthio binding pocket but none possessing a carboxylate moiety. The *Ec*MTAN formed complexes with two different methyl-Immucillin inhibitors: BnT-DADMeImmA (PDB entry 3DF9) and (4-chlorophenyl)-

thio-DADMe-ImmA (PDB entry 3O4V). These structures show that the phenyl moieties bind in the same location but possess slightly different orientations, which results from differences in the conformation of the pyrrolidine moieties of these transition-state analogues. In the 3DF9 structure, the phenyl moiety forms a herringbone interaction with the residue analogous to F107 and overlaps with the position of the α-amino moiety of SAH when bound to *Hp*MTAN. However, in 3O4V, the chlorophenyl moiety does not form any π–π stacking interactions between the inhibitor and the 5′-alkylthio binding pocket, suggesting that other interactions are predominating and forcing an alternative inhibitor conformation or the presence of the chlorine atom coupled to the phenyl moiety is sterically hindering the π–π stacking interaction.

The *Hp*MTAN–ligand interactions observed within the 5′-alkylthio binding subsite differ markedly from those observed in the analogous region of the human MTAP–methylthio-Immucillin-A complex structure (PDB entry 1K27).[38] The structural differences between *Ec*MTAN and human MTAP have been previously detailed.[28] This comparison clearly showed that MTAP has a truncated, hydrophobic 5′-alkylthio binding pocket that can accommodate a methylthio moiety but lacks sufficient volume to accommodate longer or bulkier 5′ substituents. In contrast, bacterial MTANs possess a longer 5′-alkylthio binding pocket that extends to the protein surface, which would allow for the binding of compounds with a more hydrophilic and significantly larger 5′ substituent. This is also true for *Hp*MTAN, but the structures described here shine new light on the importance of these differences.

While the 5′-alkylthio binding pockets of *Hp*MTAN and human MTAP each possess similar residues in the 5′-alkylthio binding pockets, the relative positions of these residues are significantly different (Figure 4C). H137, V135, and L279 of human MTAP form the end of the 5′-alkyl binding pocket and form primarily van der Waals interactions with the methylthio moiety of methylthio-Immucillin-A. From the superposition, it is clear that there is not sufficient volume in the human MTAP active site to accommodate the larger 5′-homocysteine moiety, which extends roughly 4.5 Å beyond the boundary of the MTAP active site surface. Additional evidence of possible steric hindrance in this region comes from the relative positions of the sulfur atoms in the two ligands. The sulfur of SAH abuts the MTAP active site envelope, whereas the sulfur of the Immucillin is positioned near the center of the 5′-alkylthio binding subsite because of a roughly 110° difference in the 4′–5′ dihedral. This suggests that the design of an inhibitor with a fixed structure at the 5′-carbon of ribose that approximates the conformation of SAH in the *Hp*MTAN–SAH complex structure should be quite selective for *Hp*MTAN.

5′-Alkylthiol Binding Pocket–Homocysteine Interactions Affect *Hp*MTAN Kinetics. The data presented here suggest a role for the *Hp*MTAN 5′-alkylthio binding subsite in specifically coordinating the homocysteine moiety of SAH and suggest that the structure of the 5′-alkylthio binding region is independent of substrate identity. Because these interactions

play an important role in substrate recognition and the structural evidence suggests that the homocysteine moiety contributes only a minor conformational entropy penalty to binding, it is expected that evidence of the impact on substrate binding could be observed using steady-state kinetics. In particular, the three additional interactions formed between HpMTAN and the SAH substrate should produce a lower K_M for the HpMTAN−SAH reaction than for the HpMTAN−MTA reaction.

To perform these experiments, we monitored the hydrolysis of either MTA or SAH by wt-HpMTAN by measuring the absorbance decrease at 274 nm. Fitting the initial velocity data allowed calculation of the kinetic parameters (Figure 4D). The K_M values for SAH and MTA were 10 ± 1 and 39 ± 5 μM, respectively (Table 2). The k_{cat} values for SAH and MTA were 1.8 ± 0.1 and 3.8 ± 0.2 s^{-1}, respectively. These values are in accordance with those determined for wild-type *Streptococcus pneumoniae* MTAN, where Singh et al. showed that wild-type *S. pneumoniae* MTAN has a 1.8-fold lower K_M when using SAH versus using MTA.[38] However, results for both HpMTAN and *S. pneumoniae* MTAN contrast with those observed for *Ec*MTAN.[39] Lee et al. showed that wt-*Ec*MTAN exhibits a 1.6-fold lower K_M when using MTA than when using SAH as the substrate, but k_{cat} values are similar for each substrate (2.6 ± 0.1 and 3.0 ± 0.1 s^{-1}), resulting in slightly higher enzymatic efficiency when using MTA as a substrate.[39]

The reason for the discrepancy in the kinetic parameters is not clear. The kinetics of the *S. pneumoniae* MTAN are more like those of HpMTAN than those of *Ec*MTAN. However, both *S. pneumoniae* MTAN and *Ec*MTAN possess a tyrosine at the corresponding position of HpMTAN H109.[39] Therefore, the difference in kinetics observed in various bacterial MTANs cannot be simply ascribed to an increase in the positive electrostatic potential due to the presence of H109 in the HpMTAN active site. Another factor potentially contributing to the kinetic differences may stem from solvent effects in the different 5′-alkylthio binding pockets. This was previously suggested by Thomas et al. to explain the large entropic and enthalpic variation observed when testing a panel of inhibitors to various bacterial MTANs.[40] That rationale may apply to data presented here. In other protein−ligand systems, the effects of ligand and active site desolvation have been tested experimentally for both hydrophilic and hydrophobic substrate/ligand binding sites, and the conclusions can be applied to the 5′-alkylthio binding subsite of MTAN.[41] Considering that the portion of the HpMTAN 5′-alkylthio binding pocket that interacts with the α-carboxyl and α-amino moieties of SAH is generally hydrophilic, the primary driving force for binding likely stems from the favorable entropy caused by ligand desolvation and active site desolvation of the hydrophilic portion of the active site. This is displayed clearly in Figure 4B, where two ordered water molecules in the MTA complex that exhibit a rather extensive hydrogen-bonded network superimpose with portions of the SAH molecule in the SAH complex. Displacement of these ordered waters affords an entropic gain, but enthalpic changes are likely minimal because of the maintenance of the specific ionic and hydrogen bonding interactions following SAH binding.

To quantify the effect of these interactions within the HpMTAN 5′-alkylthio binding pocket, we performed kinetic studies using two single mutants, F107A and H109A (Table 2). As predicted from the crystal structure, the K_M values of both mutants exhibit a minor increase (1.9-fold for F107A and 1.4-

fold for H109A) when using SAH as a substrate, while the K_M remains unchanged when using MTA. This indicates that the cation−π interaction of F107 and the ionic interaction of H109 play a role in recognizing the homocysteine moiety of SAH. Similarly, studies of *Ec*MTAN showed that mutants F105A (F107 in wt-HpMTAN) and Y107F (H109 in wt-HpMTAN) exhibited 4- and 1.3-fold increases, respectively, in the K_M values for SAH, suggesting these interactions in the 5′-alkylthio binding pocket are common features among different bacterial MTANs.[39] The effects of the F107A and H109A mutations on the k_{cat} values are more difficult to interpret. When compared to that of wt-HpMTAN, the k_{cat} values for F107A and H109A using either SAH or MTA as the substrate decreased by 3−4-fold. We did not anticipate that the catalytic rate when using MTA as a substrate would be affected. A possible rationale for the effect on the turnover rate is that the structure of the loop containing F107 and H109 is altered in the mutants, which could affect the turnover of either SAH or MTA substrates.

■ CONCLUSIONS

Characterizing interactions between the enzyme and substrate are at the heart of understanding substrate specificity and enzyme catalysis. For the bacterial MTANs, the interactions within the adenine and ribose subsites are well-documented. This study offers the first description of the specific bonding interactions between the 5′-alkylthio binding subsite of any MTAN and a homocysteine-containing ligand by determining the X-ray crystal structure of a binary complex of an inactive HpMTAN mutant with SAH and the structure of a ternary, product complex. These structures not only highlight previously unobserved interactions between the enzyme and either substrate or product but also show that this portion of the enzyme active site is invariant with respect to its substrate-bound state and substrate identity. Additionally, the wt-HpMTAN−SRH−adenine ternary complex structure shows that the interactions between the homocysteine moiety and the enzyme active site are consistent with those observed for the HpMTAN-D198N−SAH complex. The 4-fold lower K_M and the 2-fold lower k_{cat} observed when using SAH as a substrate versus MTA reflect the additional interactions between the 5′-alkylthio binding subsite and the homocysteine moiety of either the substrate or product. Taken together, these results suggest that the 5′-alkylthio binding subsite is a prime target for the design of new MTAN inhibitors that are highly specific to bacterial MTANs but will selectively kill *H. pylori* while sparing beneficial commensal bacteria endogenous to the human gastrointestinal tract.

■ AUTHOR INFORMATION

Corresponding Author
*Department of Chemistry, University of Toledo, 2801 W. Bancroft St., Toledo, OH 43606. Telephone: (419) 530-1585. Fax: (419) 530-4033. E-mail: donald.ronning@utoledo.edu.

Author Contributions
The manuscript was written through contributions of all authors. All authors have given approval to the final version of the manuscript.

Notes
The authors declare no competing financial interest.

■ ABBREVIATIONS

MTAN, 5′-methylthioadenosine/*S*-adenosylhomocysteine nucleosidase; SAH, *S*-adenosylhomocysteine; MTA, 5′-methylthioadenosine; 5′-DOA, 5′-deoxyadenosine; SAM, *S*-adenosylmethionine; AI1, autoinducer I; AI2, autoinducer II; SRH, *S*-ribosylhomocysteine; AHL, *N*-acylhomoserine lactone; MTAP, 5′-MTA phosphorylase; *Hp*MTAN, *H. pylori* MTAN; *Ec*MTAN, *E. coli* MTAN; GABA, γ-aminobutyric acid; AChBP, acetylcholine binding protein.

■ REFERENCES

(1) Choi-Rhee, E. J., and Cronan, J. E. (2005) A nucleosidase required for in vivo function of the S-adenosyl-L-methionine radical enzyme, biotin synthase. *Chem. Biol. 12*, 589−593.

(2) Della Ragione, F., Porcelli, M., Carteni-Farina, M., Zappia, V., and Pegg, A. E. (1985) *Escherichia coli* S-adenosylhomocysteine/5′-methylthioadenosine nucleosidase. Purification, substrate specificity and mechanism of action. *Biochem. J. 232*, 335−341.

(3) Miller, C. H., and Duerre, J. A. (1968) S-ribosylhomocysteine cleavage enzyme from *Escherichia coli*. *J. Biol. Chem. 243*, 92−97.

(4) Sufrin, J. R., Meshnick, S. R., Spiess, A. J., Garofalo-Hannan, J., Pan, X. Q., and Bacchi, C. J. (1995) Methionine recycling pathways and antimalarial drug design. *Antimicrob. Agents Chemother. 39*, 2511−2515.

(5) Borchardt, R. T. (1980) S-Adenosyl-L-methionine-dependent macromolecule methyltransferases: Potential targets for the design of chemotherapeutic agents. *J. Med. Chem. 23*, 347−357.

(6) Pajula, R. L., and Raina, A. (1979) Methylthioadenosine, a potent inhibitor of spermine synthase from bovine brain. *FEBS Lett. 99*, 343−345.

(7) Parveen, N., and Cornell, K. A. (2011) Methylthioadenosine/S-adenosylhomocysteine nucleosidase, a critical enzyme for bacterial metabolism. *Mol. Microbiol. 79*, 7−20.

(8) Fong, K. P., Chung, W. S. O., Lamont, R. J., and Demuth, D. R. (2001) Intra- and interspecies regulation of gene expression by *Actinobacillus actinomycetemcomitans* LuxS. *Infect. Immun. 69*, 7625−7634.

(9) Vendeville, A., Winzer, K., Heurlier, K., Tang, C. M., and Hardie, K. R. (2005) Making 'sense' of metabolism: Autoinducer-2, LuxS and pathogenic bacteria. *Nat. Rev. Microbiol. 3*, 383−396.

(10) Marques, J. C., Lamosa, P., Russell, C., Ventura, R., Maycock, C., Semmelhack, M. F., Miller, S. T., and Xavier, K. B. (2011) Processing the interspecies quorum-sensing signal autoinducer-2 (AI-2): Characterization of phospho-(S)-4,5-dihydroxy-2,3-pentanedione isomerization by LsrG protein. *J. Biol. Chem. 286*, 18331−18343.

(11) Fuqua, C., and Greenberg, E. P. (2002) Listening in on bacteria: Acyl-homoserine lactone signalling. *Nat. Rev. Mol. Cell Biol. 3*, 685−695.

(12) Li, X., Apel, D., Gaynor, E. C., and Tanner, M. E. (2011) 5′-Methylthioadenosine Nucleosidase Is Implicated in Playing a Key Role in a Modified Futalosine Pathway for Menaquinone Biosynthesis in *Campylobacter jejuni*. *J. Biol. Chem. 286*, 19392−19398.

(13) Hiratsuka, T., Furihata, K., Ishikawa, J., Yamashita, H., Itoh, N., Seto, H., and Dairi, T. (2008) An alternative menaquinone biosynthetic pathway operating in microorganisms. *Science 321*, 1670−1673.

(14) Seto, H., Jinnai, Y., Hiratsuka, T., Fukawa, M., Furihata, K., Itoh, N., and Dairi, T. (2008) Studies on a new biosynthetic pathway for menaquinone. *J. Am. Chem. Soc. 130*, 5614−5615.

(15) Wang, S., Haapalainen, A. M., Yan, F., Du, Q., Tyler, P. C., Evans, G. B., Rinaldo-Matthis, A., Brown, R. L., Norris, G. E., Almo, S. C., and Schramm, V. L. (2012) A Picomolar Transition State Analogue Inhibitor of MTAN as a Specific Antibiotic for *Helicobacter pylori*. *Biochemistry 51*, 6892−6894.

(16) Lee, J. E., Cornell, K. A., Riscoe, M. K., and Howell, P. L. (2001) Structure of *E. coli* 5′-methylthioadenosine/S-adenosylhomocysteine nucleosidase reveals similarity to the purine nucleoside phosphorylases. *Structure 9*, 941−953.

(17) Park, E. Y., Oh, S. I., Nam, M. J., Shin, J. S., Kim, K. N., and Song, H. K. (2006) Crystal structure of 5′-methylthioadenosine nucleosidase from *Arabidopsis thaliana* at 1.5-angstrom resolution. *Proteins 65*, 519−523.

(18) Ronning, D. R., Iacopelli, N. M., and Mishra, V. (2010) Enzyme-ligand interactions that drive active site rearrangements in the *Helicobacter pylori* 5′-methylthioadenosine/S-adenosylhomocysteine nucleosidase. *Protein Sci. 19*, 2498−2510.

(19) Siu, K. K., Lee, J. E., Smith, G. D., Horvatin-Mrakovcic, C., and Howell, P. L. (2008) Structure of *Staphylococcus aureus* 5′-methylthioadenosine/S-adenosylhomocysteine nucleosidase. *Acta Crystallogr. F64*, 343−350.

(20) Allart, B., Gatel, M., Guillerm, D., and Guillerm, G. (1998) The catalytic mechanism of adenosylhomocysteine/methylthioadenosine nucleosidase from *Escherichia coli*: Chemical evidence for a transition state with a substantial oxocarbenium character. *Eur. J. Biochem. 256*, 155−162.

(21) Cornell, K. A., Swarts, W. E., Barry, R. D., and Riscoe, M. K. (1996) Characterization of recombinant *Escherichia coli* 5′-methylthioadenosine/S-adenosylhomocysteine nucleosidase: Analysis of enzymatic activity and substrate specificity. *Biochem. Biophys. Res. Commun. 228*, 724−732.

(22) Lee, J. E., Cornell, K. A., Riscoe, M. K., and Howell, P. L. (2003) Structure of *Escherichia coli* 5′-methylthioadenosine/S-adenosylhomocysteine nucleosidase inhibitor complexes provide insight into the conformational changes required for substrate binding and catalysis. *J. Biol. Chem. 278*, 8761−8770.

(23) Lee, J. E., Smith, G. D., Horvatin, C., Huang, D. J. T., Cornell, K. A., Riscoe, M. K., and Howell, P. L. (2005) Structural snapshots of MTA/AdoHcy nucleosidase along the reaction coordinate provide insights into enzyme and nucleoside flexibility during catalysis. *J. Mol. Biol. 352*, 559−574.

(24) Guan, R., Ho, M. C., Brenowitz, M., Tyler, P. C., Evans, G. B., Almo, S. C., and Schramm, V. L. (2011) Entropy-Driven Binding of Picomolar Transition State Analogue Inhibitors to Human 5′-Methylthioadenosine Phosphorylase. *Biochemistry 50*, 10408−10417.

(25) Longshaw, A. I., Adanitsch, F., Gutierrez, J. A., Evans, G. B., Tyler, P. C., and Schramm, V. I. (2010) Design and Synthesis of Potent "Sulfur-Free" Transition State Analogue Inhibitors of 5′-Methylthioadenosine Nucleosidase and 5′-Methylthioadenosine Phosphorylase. *J. Med. Chem. 53*, 6730−6746.

(26) Lee, J. E., Singh, V., Evans, G. B., Tyler, P. C., Furneaux, R. H., Cornell, K. A., Riscoe, M. K., Schramm, V. L., and Howell, P. L. (2005) Structural rationale for the affinity of pico- and femtomolar transition state analogues of *Escherichia coli* 5′-methylthioadenosine/S-adenosylhomocysteine nucleosidase. *J. Biol. Chem. 280*, 18274−18282.

(27) Gutierrez, J. A., Luo, M., Singh, V., Li, L., Brown, R. L., Norris, G. E., Evans, G. B., Furneaux, R. H., Tyler, P. C., Painter, G. F., Lenz, D. H., and Schramm, V. L. (2007) Picomolar inhibitors as transition-state probes of 5′-methylthioadenosine nucleosidases. *ACS Chem. Biol. 2*, 725−734.

(28) Lee, J. E., Settembre, E. C., Cornell, K. A., Riscoe, M. K., Sufrin, J. R., Ealick, S. E., and Howell, P. L. (2004) Structural comparison of MTA phosphorylase and MTA/AdoHcy nucleosidase explains substrate preferences and identifies regions exploitable for inhibitor design. *Biochemistry 43*, 5159−5169.

(29) Otwinowski, Z., and Minor, W. (1997) Processing of X-ray diffraction data collected in oscillation mode. *Methods Enzymol. 276*, 307−326.

(30) Kissinger, C. R., Gehlhaar, D. K., and Fogel, D. B. (1999) Rapid automated molecular replacement by evolutionary search. *Acta Crystallogr. D55*, 484−491.

(31) Adams, P. D., Afonine, P. V., Bunkoczi, G., Chen, V. B., Davis, I. W., Echols, N., Headd, J. J., Hung, L. W., Kapral, G. J., Grosse-Kunstleve, R. W., McCoy, A. J., Moriarty, N. W., Oeffner, R., Read, R. J., Richardson, D. C., Richardson, J. S., Terwilliger, T. C., and Zwart, P. H. (2010) PHENIX: A comprehensive Python-based system for macromolecular structure solution. *Acta Crystallogr. D66*, 213−221.

(32) Adams, P. D., Gopal, K., Grosse-Kunstleve, R. W., Hung, L. W., Ioerger, T. R., McCoy, A. J., Moriarty, N. W., Pai, R. K., Read, R. J., Romo, T. D., Sacchettin, J. C., Sauter, N. K., Storoni, L. C., and Terwilligerf, T. C. (2004) Recent developments in the PHENIX software for automated crystallographic structure determination. *J. Synchrotron Radiat. 11*, 53−55.

(33) Emsley, P., Lohkamp, B., Scott, W. G., and Cowtan, K. (2010) Features and development of Coot. *Acta Crystallogr. D66*, 486−501.

(34) Lummis, S. C. R., McGonigle, I., Ashby, J. A., and Dougherty, D. A. (2011) Two Amino Acid Residues Contribute to a Cation-π Binding Interaction in the Binding Site of an Insect GABA Receptor. *J. Neurosci. 31*, 12371−12376.

(35) Brejc, K., van Dijk, W. J., Klaassen, R. V., Schuurmans, M., van der Oost, J., Smit, A. B., and Sixma, T. K. (2001) Crystal structure of an ACh-binding protein reveals the ligand-binding domain of nicotinic receptors. *Nature 411*, 269−276.

(36) Dougherty, D. A. (1996) Cation-π interactions in chemistry and biology: A new view of benzene, Phe, Tyr, and Trp. *Science 271*, 163−168.

(37) Siu, K. K. W., Asmus, K., Zhang, A. N., Horvatin, C., Li, S., Liu, T., Moffatt, B., Woods, V. L., Jr., and Howell, P. L. (2011) Mechanism of substrate specificity in 5′-methylthioadenosine/S-adenosylhomocysteine nucleosidases. *J. Struct. Biol. 173*, 86−98.

(38) Singh, V., Shi, W., Evans, G. B., Tyler, P. C., Furneaux, R. H., Almo, S. C., and Schramm, V. L. (2004) Picomolar transition state analogue inhibitors of human 5′-methylthioadenosine phosphorylase and X-ray structure with MT-immucillin-A. *Biochemistry 43*, 9−18.

(39) Lee, J. E., Luong, W., Huang, D. J. T., Cornell, K. A., Riscoe, M. K., and Howell, P. L. (2005) Mutational analysis of a nucleosidase involved in quorum-sensing autoinducer-2 biosynthesis. *Biochemistry 44*, 11049−11057.

(40) Thomas, K., Haapalainen, A. M., Burgos, E. S., Evans, G. B., Tyler, P. C., Gulab, S., Guan, R., and Schramm, V. L. (2012) Femtomolar Inhibitors Bind to 5′-Methylthioadenosine Nucleosidases with Favorable Enthalpy and Entropy. *Biochemistry 51*, 7541−7550.

(41) Syme, N. R., Dennis, C., Bronowska, A., Paesen, G. C., and Homans, S. W. (2010) Comparison of entropic contributions to binding in a "hydrophilic" versus "hydrophobic" ligand-protein interaction. *J. Am. Chem. Soc. 132*, 8682−8689.